**Symposium "Experimental Fluid Mechanics"**
7.–9. September 2021, Bremen

# The von Kármán Vortex Street, an archetype for Machine Learning in turbulence

**Mohammad Sharifi Ghazijahani, Florian Heyder, Jörg Schumacher, Christian Cierpka**
Institute for Thermodynamics and Fluid Mechanics, Technische Universität Ilmenau, P.O. 100565, 98684 Ilmenau

Machine Learning, Vortex shedding, wake flows, von Kármán Vortex Street

## Abstract

The application of machine learning provides many opportunities due to its substantial advantage in dealing with large data sets [Pandey et al. 2020]. It is of particular interest for the prediction of turbulent flows. Within this context, echo state networks as a type of machine learning algorithms with recurrent networks, are very efficient in predicting the temporal behavior of dynamic systems after a supervised learning process. In this regard, the von Kármán vortex street is a suitable candidate for training and testing the echo state network prior to its application to more chaotic turbulent fields due to its thoroughly investigated flow field and semi two-dimensionality for low Reynolds numbers. Therefore, we implement echo state networks for the prediction of the velocity fields in a von Kármán vortex street using Particle Image Velocimetry (PIV) data. The data is reduced by Proper Orthogonal Decomposition (POD), and the flow is reconstructed by the first hundred most energetic modes. Then, an echo state network with 3000 neurons is trained for 700 time steps, and optimized for its main hyperparameters to reach maximal performance. The predictions are selected based on their capabilities of predicting the vertical velocity direction. The optimized set is capable of predicting the flow qualitatively in terms of upward and downward passing streams but fails for their magnitude estimation. Therefore, further investigations are required from quantitative point of view.

## Introduction

Machine Learning (ML) algorithms can be used for the prediction of complex systems like turbulent flows [Pandey et al. 2020]. These algorithms are in particular very efficient in dealing with large data sets in terms of computation cost and time. On the other hand, large volumes of experimental and numerical data are becoming an inseparable part of fluid dynamic studies. Meanwhile, the continuous advances in computer capabilities make ML implementations cheaper and more convenient. Thus, ML applications in fluid dynamics have gained significant attention in recent years. Turbulent flow prediction is one of the main aspirations of fluid dynamics, where ML application show promising advantages by understanding the flow physics and statistical and geometrical patterns of turbulence.

On this subject, the prediction of von Kármán Vortex Street (KVS), as the vortex shedding in the flow passing a cylinder, can be a suitable case study. KVS is a well-known example of a turbulent flow, with a thoroughly studied semi-two-dimensional flow field for low Reynolds numbers. The shedding process starts at $Re \approx 90$. The vortex shedding frequency, represented by the Strouhal number (St), rises as Re increases. Then, for $400<Re<6000$, the St


GALA e.V., Karlsruhe, Germany, ISBN 978-3-9816764-7-1

has a constant value of about 0.22 [Lienhard 1966]. Recently, several attempts were made to control or predict the KVS by ML implementations. Rabault et al. [Rabault et al. 2018] achieved active flow control over KVS by Deep Reinforcement Learning (DRL). They minimized the drag through reduction of vortex shedding strength at Re = 100. Schena [Schena 2021] compared two ML techniques, DRL and Bayesian Optimization, for flow control of KVS at Re=100. Morast [Morast 2019] implemented deep learning to identify the Reynolds number and the location of the cylinder in KVS. Moreover, Arntzen [Arntzen 2019] used ML for velocity field prediction in KVS at 2500<Re<6000. He used sparse-dynamic-mode-decomposition scaling relations of the velocity field instead of POD-Interpolation approach, which resulted in predictions with less error.

A class of ML approaches for the prediction of complex systems are RNN. These networks have recurrent connections between their nodes, which allows them to remember the past and influence the future. Thus, they are very suitable for learning from time series and exhibit temporal behaviors. Echo State Networks (ESN) as a subtype of RNN consists of a reservoir with fixed recurrent connections that receives the input, then only the readout matrix of neuron states are trained to reach the best output with minimum error. A schematic sketch of such an architecture is shown in Figure 1. ESNs can describe the evolution of dynamic systems without solving the underlying equations. Thus, they are of particular interest for dynamic flow prediction and were already successfully applied to two-dimensional moist Rayleigh-Bénard convection [Heyder et al. 2021].

In this study, we aim at the prediction of the velocity field of KVS by an ESN implementation. First, experimental data of KVS flow fields is obtained by PIV measurements. Then, the data was reduced by POD. The first hundred most energetic modes in terms of kinetic energy of POD were considered for supervised learning of the ESN. However, it may also be better to calculate the POD modes by the vorticity fields. Thus, they are optimal in terms of entropy, which was shown to be beneficial by Kostas et al. [Kostas et al. 2005] and later also Cierpka et al. [Cierpka et al. 2010] for momentum transfer. Finally, we optimized the hyperparameters of the ESN to reach the best possible prediction.

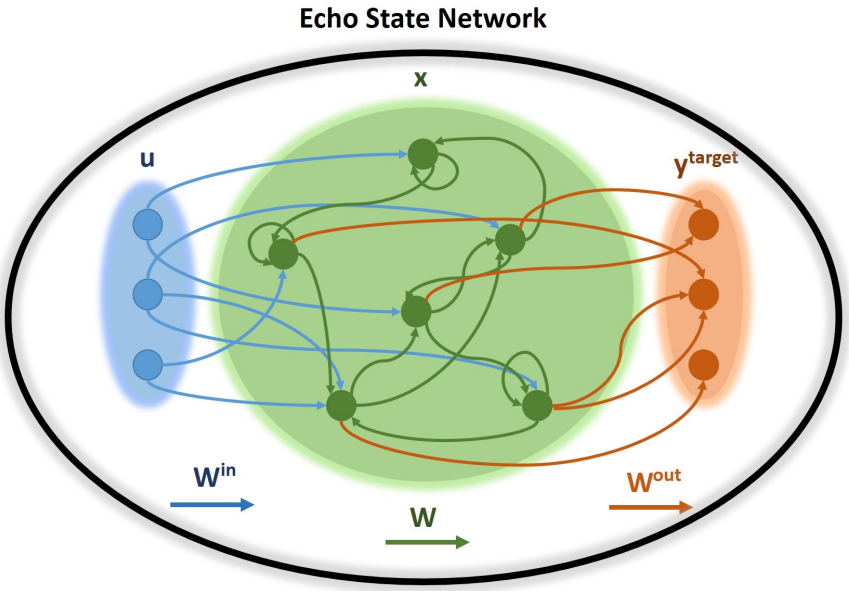


Fig. 1: A schematic sketch of an Echo State Network (ESN).


GALA e.V., Karlsruhe, Germany, ISBN 978-3-9816764-7-1

## Methods

PIV measurements of the flow around a cylinder (diameter = 8 mm) were performed in a water channel with a cross section of 50 × 50 mm$^2$. The flow was seeded by Polyamide particles with a diameter of 20 µm. A camera (HS 4M by LaVision GmbH) was used to capture the images of the flow field illuminated by a continuous wave laser. The Reynolds number based on the cylinder diameter was 900. For the PIV measurements five different recording frequencies (F) of 400, 100, 50, 25, and 12.5 Hz for a measurement time of 25, 50, 100, 200, and 400 seconds respectively were used. For a St of 0.22 this results to 83, 165, 330, 660 vortex shedding events and a temporal resolution, $t/t_{characteristic}$, of 120, 30, 15, 7.5, 3 time steps per vortex shedding event, respectively. This ensures the possibility of training and testing the algorithms with different temporal resolutions and time spans. The experimental setup and the average velocity magnitude field are shown in Figures 2 and 3, respectively. The flow is illuminated by a laser sheet parallel to the side walls of the channel, and the images are captured by a camera located outside the water channel perpendicular to the laser sheet. In the averaged velocity field the symmetric wake after the cylinder is the footprint of vortex shedding while also the growing boundary layers near the walls are apparent.

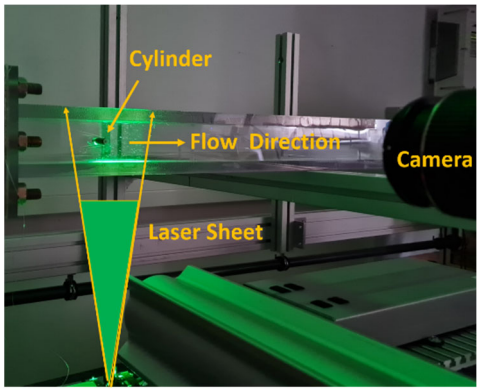


Fig. 2: Experimental Setup.

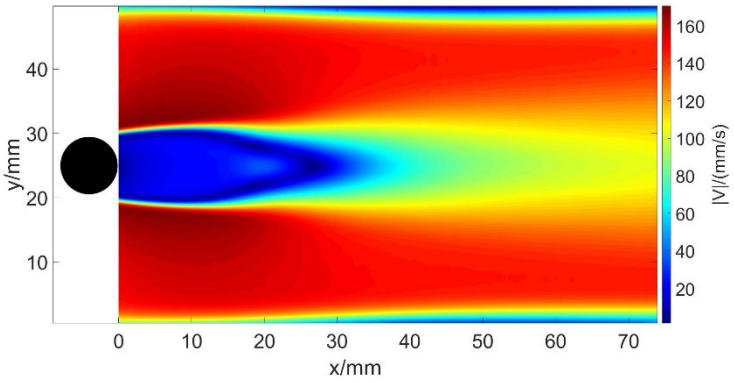


Fig. 3: Average flow field for 50 Hz.

In this study, an ESN was implemented to predict the flow. The weight matrix of its recurrent connections (W) and the input weights ($W^{in}$) were selected randomly at the beginning. Figure 1 is a schematic sketch of an ESN with its corresponding W and $W^{in}$ as the blue and green vectors. Then the output weights ($W^{out}$) were optimized during a supervised learning process by feeding training data to the system. Finally, this trained reservoir predicted the flow.

ESNs are fed by an input signal $u(n) \in R^{Nu}$ corresponding to a desired target output signal $y^{target}(n)$ for some discrete time steps n=1, …, T. Then the reservoir predicts an output $y(n) \in R^{Ny}$ and tries to minimize an error $E(y,y^{target})$ in this case the Root-Mean-Square Error (RMSE):

$$E(y, y^{target}) = \frac{1}{N_y}\sum_{i=1}^{Ny}\sqrt{\frac{1}{T}\sum_{n=1}^{T}\left(y_i(n) - {y_i}^{target}(n)\right)^2} \qquad (1)$$

The neurons are updated by Equations 2 and 3. α is the leaking rate and describes some kind of blending between the old state x and its update $\tilde{x}$. The output signals are collected in a linear readout layer by a $W^{out}$ readout weight matrix. As mentioned before, W and $W^{in}$ are preselected randomly while $W^{out}$ is chosen by Equation 5.


GALA e.V., Karlsruhe, Germany, ISBN 978-3-9816764-7-1

$$\tilde{x}(n) = \tanh\left(W^{in}[1; u(n)\right] + Wx(n-1)) \quad (2)$$

$$x(n) = (1-\alpha)x(n-1) + \alpha\tilde{x}(n) \quad (3)$$

$$y(n) = W^{out}[1; u(n); x(n)] \quad (4)$$

$$W^{out} = arg\ min \frac{1}{N}\sum_{n=1}^{N_y}(\sum_{n=1}^{T}\left(y_i(n) - {y_i}^{target}(n)\right)^2 + \beta\|w_i^{out}\|^2) \quad (5)$$

The reservoir is defined by ($W^{in}$, W, α), and the variables that can control these three are called hyperparameters, Three of them have higher importance according to the literature [Lukoševičius 2012], input scaling, leaking rate, and spectral radius. The input scaling is the domain in which the input weights are collected. These can be uniformly or independently set for input signals. The input scale regulates the amount of the nonlinearity of the reservoir plus the relative weight of current input against the history. The leaking rate represents the speed of reservoir update. Therefore, the flow dynamics play a central role in determining the most efficient leaking rate. Finally, the spectral radius is the maximal Eigenvalue of the W. The spectral radius should remain below one to ensure echo state properties in most situations. For this study, the ESN model was created in Python using the easyesn library for 3000 neurons. Where each neuron is sparsely connected to 20 percent of others. Then it is trained and tested for 700 time steps with different sets of hyperparameters to reach the maximum efficiency.

## Results

In Figure 4 the vertical velocity field (right) and the magnitude of the velocity field (left) are shown for a randomly chosen time step. There is a stationary region behind the cylinder followed by upward and downward directed fluid as expected for vortex shedding. Figure 3 displays the average flow field. The typical cone-like shape and boundary layers on the top and bottom wall with increasing thickness further downstream are apparent. It should be noted that the PIV results possess good quality in terms of the fraction of outlier vectors which stands below 1% for the normalized median test. Figure 5 shows a sample vector field of PIV measurement, where a low fraction of the outliers is evident. A standard correlation was applied for PIV processing for an initial rectangular interrogation window size of 64×64 with 50% overlap and a final circular window size of 16×16 with 50% overlap. The weights of initial and final interrogation windows were one and three, respectively. The final spatial resolution was 0.35×0.35 mm$^2$ in physical coordinates with 141×211 vectors. The velocities were calibrated with respect to the channel height with a final magnification magnitude of 22.7 px/mm. Further increase of spatial resolution was neglected due to the increased volume of data, which is not necessary for this study.

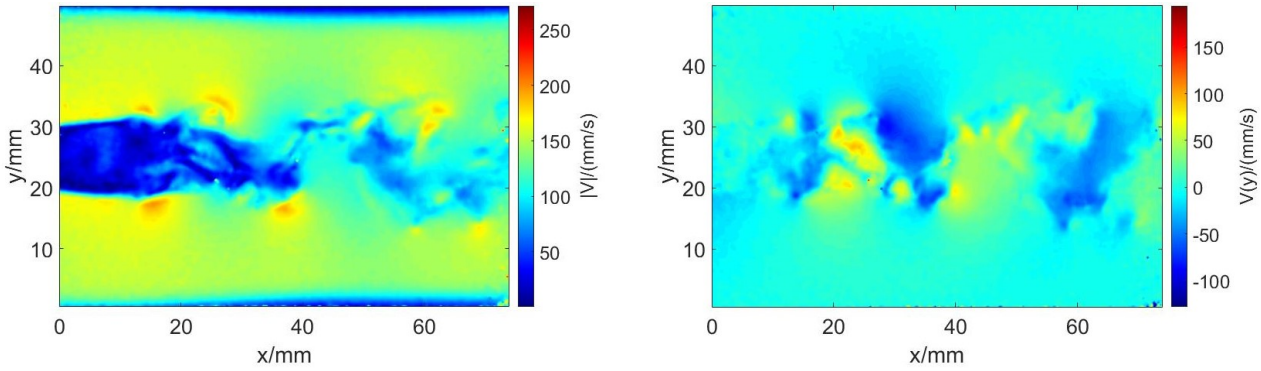


Fig. 4: Sample total (left) and vertical (right) velocity fields of PIV measurements.


GALA e.V., Karlsruhe, Germany, ISBN 978-3-9816764-7-1

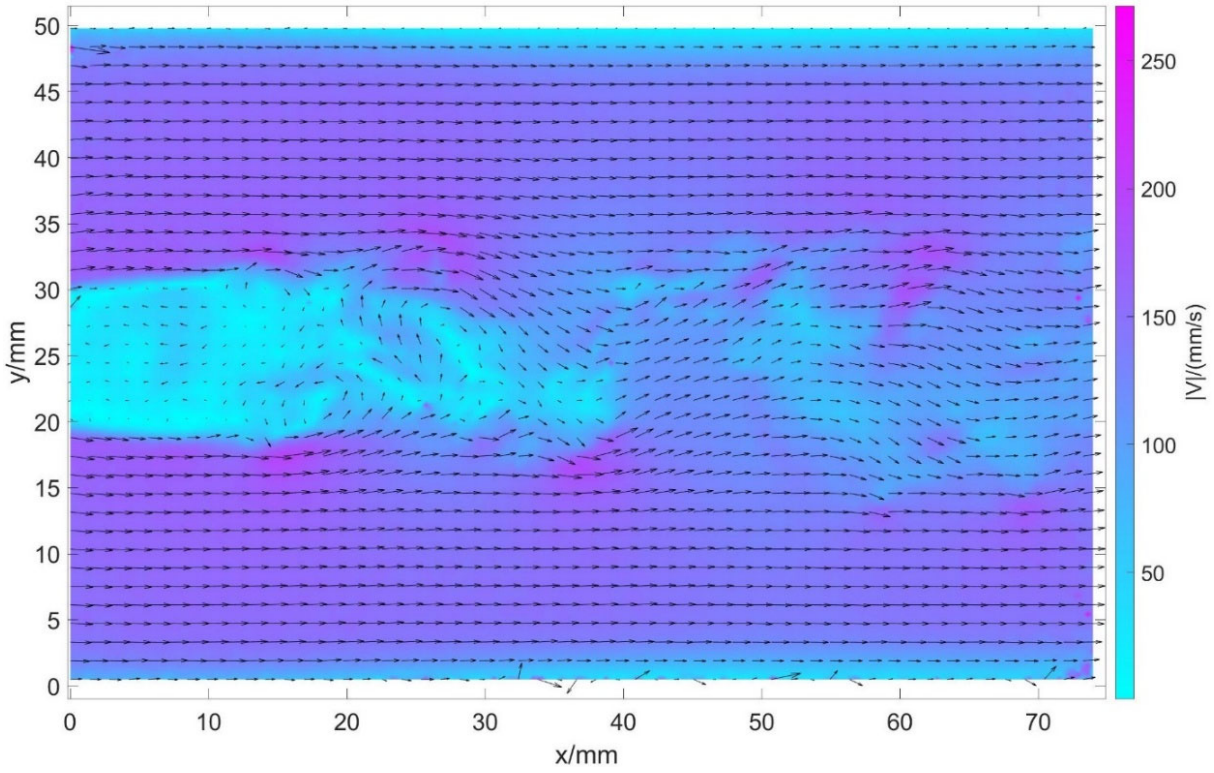


Fig. 5: A sample vector field of PIV measurement.

In order to reduce the parameter space for the networks, POD analysis was applied to the results to derive the most dominant spatial modes and their temporal coefficients in the flow field [Pandey et al. 2020, Heyder et al. 2021]. Figure 6 displays the kinetic energies of POD modes as a fraction of the total kinetic energy of the flow for F = 50 Hz. Two main modes with 15 % of total energy are evident in Figure 6, whereas the energies of the next modes drop significantly. Figure 7 shows the vertical velocity fields of the first four modes. Vertical velocities are of particular importance due to their implementation for prediction quality analysis that will be explained later. For a better understanding of the dynamic behavior of the modes, Figure 8 shows the coefficients of the first four modes of the POD analysis for 50 Hz frequency. The alternation of modes one and two represent the vortex shedding as expected and has a typical frequency of 3.3 Hz which results in a Strouhal number of 0.22. However, the spatial domains of the temporal coefficients of these two main modes are varying. Figure 9 shows this variation for mode one, which has also a periodic pattern itself. Smaller features are represented by the higher modes, where their temporal coefficients show evolutions that are more complex. For ML application, we consider only the first hundred modes with 73 % of total kinetic energy, and used these hundred modes for flow reconstruction and prediction. The corresponding reconstructed and residual fields are shown in Figure 10. The reconstructed flow field preserves the main features of the flow despite losing some of its energy to the residual flow. The best data set in terms of frequency for ML implementation is the one with sufficient temporal resolution while covering a relatively long time as well. F= 50 Hz is the best data set from this point of view. Later, other frequencies will also be used and investigated.


GALA e.V., Karlsruhe, Germany, ISBN 978-3-9816764-7-1

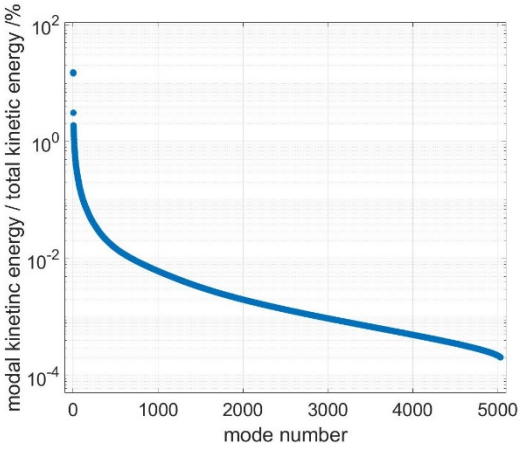


Fig. 6: Energies of eigen modes for 50 Hz.

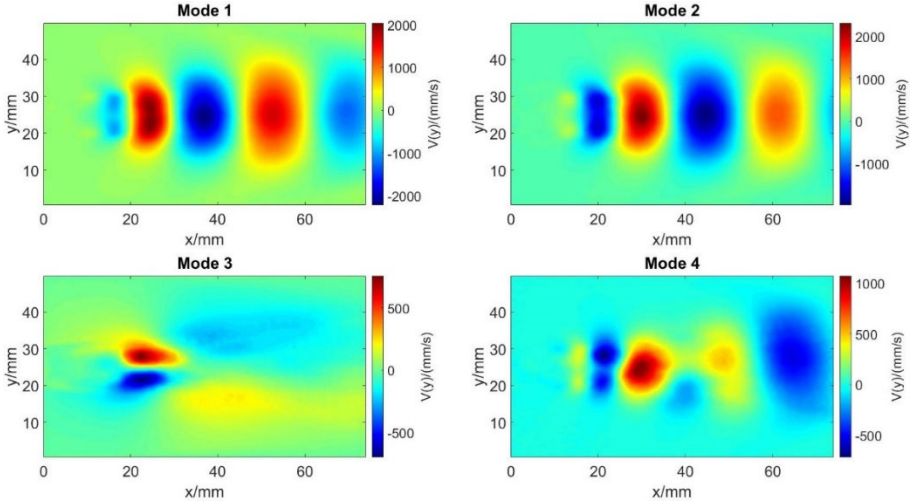


Fig. 7: Vertical velocities of modes 1, 2, 3, and 4 for 50 Hz.

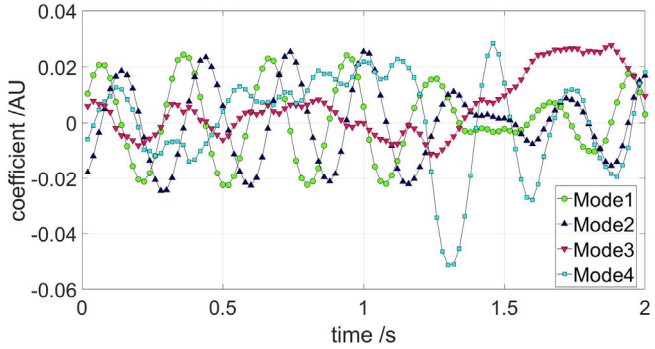


Fig. 8: Temporal coefficient values of modes 1, 2, 3, and 4 for 50 Hz.

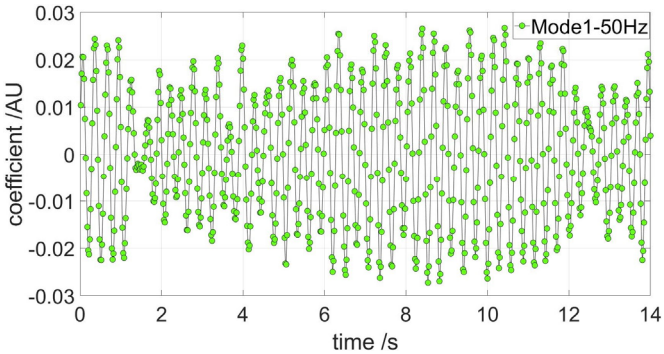


Fig. 9: Temporal coefficient values of mode one for 50 Hz.


GALA e.V., Karlsruhe, Germany, ISBN 978-3-9816764-7-1

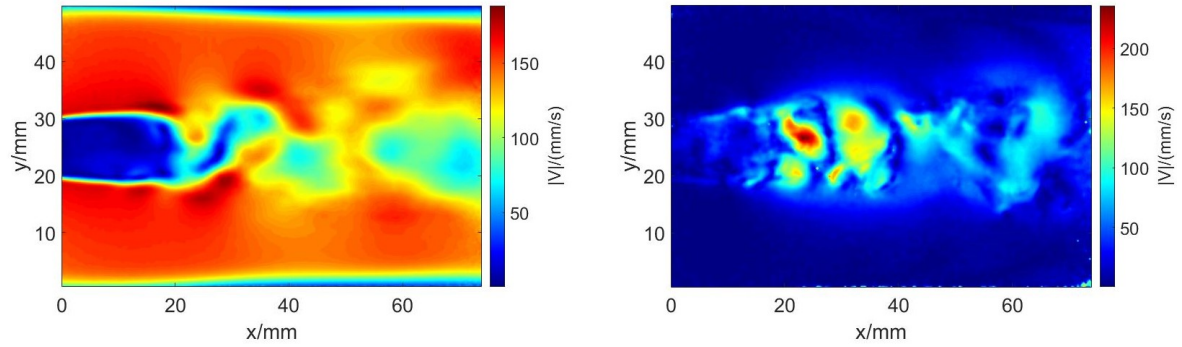


Fig. 10: Velocity field of the reconstructed flow by first hundred modes (left), and the corresponding residual field (right).

Prediction evaluation is necessary for ESN optimization. One of the typical parameters for this is Mean Square Error (MSE) of all individual velocity components. However, MSE favors predictions closer to the average flow. Figure 11 shows a sample velocity field with two predictions, a and b along with the corresponding experimental flow field indicated as c. Case a is very similar to the average field without any vortex shedding and related upward and downward flow, whereas case b is closer to the reality with distinguishable vortical features. Therefore, whatever the prediction evaluation parameter is, it should favor case b over a. However, the MSE value for case a is 582 $mm^2/s^2$ and for case b is 1023 $mm^2/s^2$. Therefore, MSE is not an ideal parameter as it always favors the predictions closer to the average flow regardless of preserving vortical structures at their correct positions. After a thorough investigation, which will be presented elsewhere, we decided to use the Vertical Velocities Prediction of Direction (VVPD) as a parameter for prediction evaluation. VVPD is defined as the ratio of correct prediction of vertical velocities in real flow with $|Vy|>17.6$ mm/s in terms of their positive or negative direction. 17.6 mm/s is equal to one pixel displacement in the PIV images, and the reason for defining it as a threshold is to neglect the displacements below one pixel, which are dominant outside the vortices. Higher VVPD values indicate better prediction of upward and downward flows. However, this parameter does not deal with the prediction of vertical velocity magnitudes.

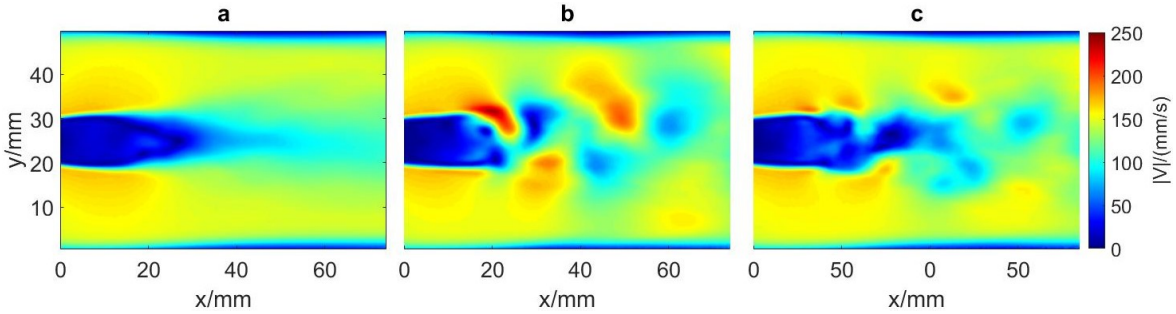


Fig. 11: Sample velocity fields of two predictions (a) and (b), and the corresponding measured velocity field (c).

Next, the hyperparameters of the ESN are optimized to reach the best prediction. For this, input scaling, spectral radius, and leaking rate are chosen as the three major hyperparameters with most influence. Figure 12 demonstrates the VVPD values versus these hyperparameters. On the left side, input scaling is changed from 0.1 to 20 for three different leaking rates = 0.8, 0.9, 0.95, while the spectral radius is fixed to 0.95. Here, VVPD values are in-


GALA e.V., Karlsruhe, Germany, ISBN 978-3-9816764-7-1

creasing substantially as the input scaling increases. They reach two peaks at input scaling = 3 and 5 and decrease afterward for all three different leaking rate values. However, maximal performance is in leaking rate = 0.95, which means a very low weight of past states in the prediction of next states. In the middle of Figure 12, the VVPD variations with respect to spectral radius are plotted for input scaling = 3, 5, and 7 and leaking rate = 0.95. The results show that as the input scaling increases, VVPD decreases and reaches its minimum values around 0.8-0.9. Then a sharp rise in VVPD is followed with its maximal value for spectral radius = 0.97 in input scaling = 3. Finally, in the right side of Figure 12 for input scaling = 3, leaking rate is varied from 0.05 to 0.99 for spectral radius = 0.5, 0.95, 0.97. Generally, VVPD rises with the increase of leaking rate, and the best performance is for leaking rate = 0.95 and spectral radius = 0.97. Therefore, the optimized set of hyperparameters is one with leaking rate = 0.95, spectral radius = 0.97 and input scaling = 3 to achieve the best performance. In order to have a deeper understanding of the performance of the optimized case, the VVPD values of this prediction and another case with similar spectral radius and input scaling but leaking rate = 0.05 are shown in Figure 13 for comparison. The overall VVPD values of the optimized case stand above 0.5 and even reaches 0.85. However, for the latter case, the VVPD values decrease significantly and remain below 0.2. Due to the phase shift in the predictions for some time steps, there are also below 0.5 VVPDs for the optimized case, which have semi-periodic nature. So, one can say that these are for times where prediction is ahead or behind the measurements. The vertical velocity fields of optimized prediction and measurements are shown in Figure 14 for time step = 25 and 400. Overall, for both cases very good predictions of vertical velocity directions are achieved. However, the magnitudes of predicted values are higher compared to reality.

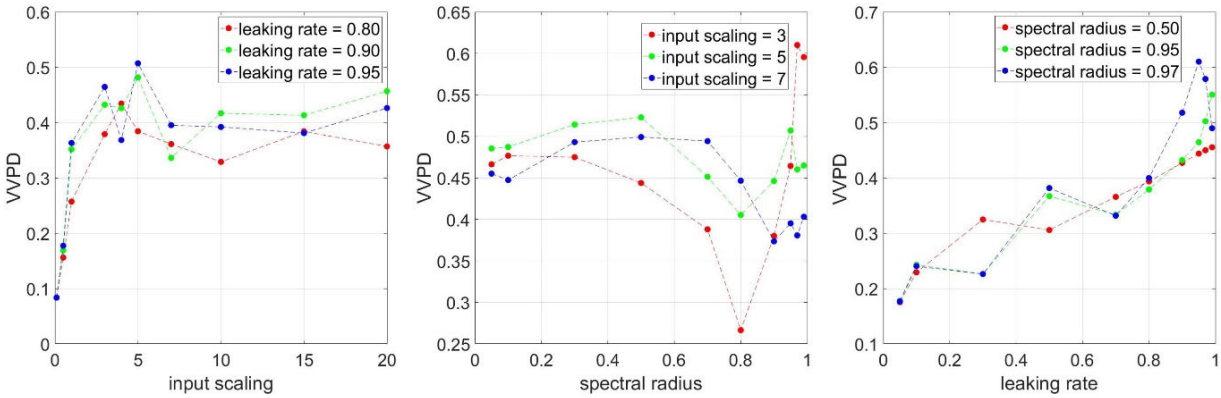


Fig. 12: VVPD (vertical velocities prediction of direction) values with respect to variations in input scaling (left), spectral radius (middle), and leaking rate (right).


GALA e.V., Karlsruhe, Germany, ISBN 978-3-9816764-7-1

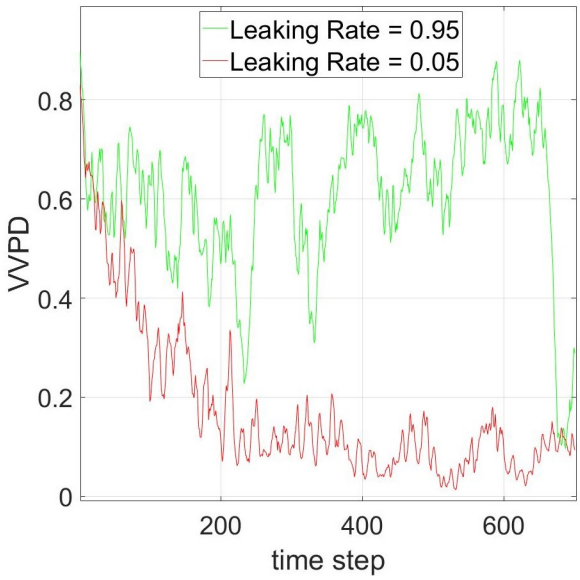


Fig. 13: VVPD values for the optimized set (green) and another set of hyperparameters (red).

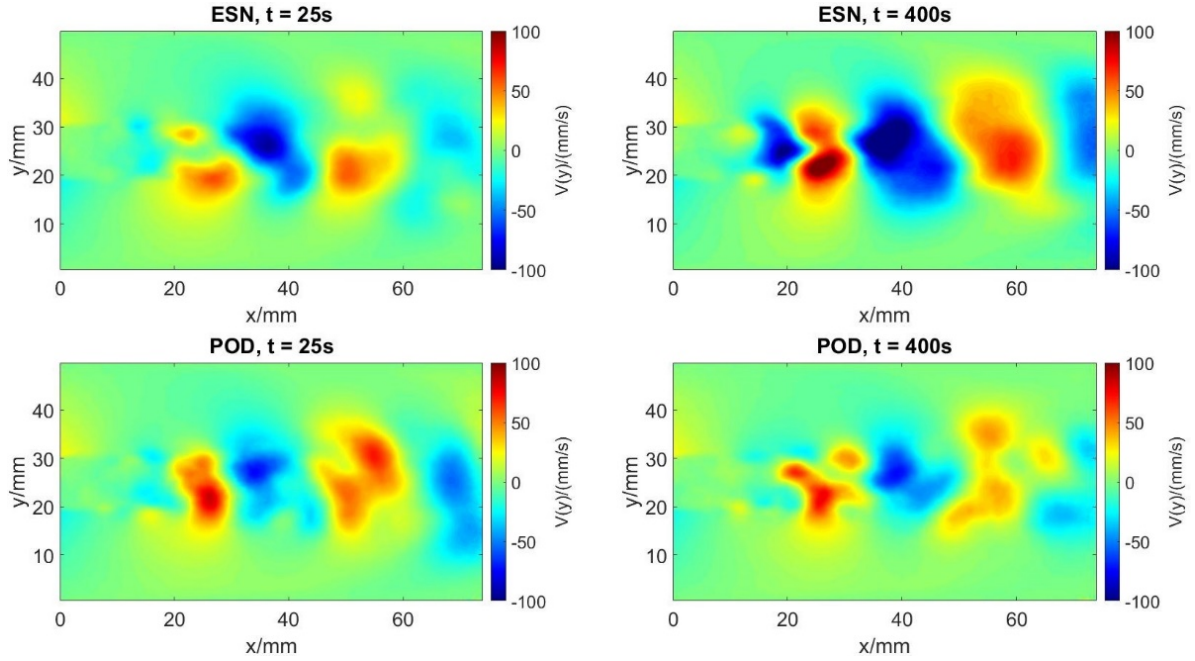


Fig. 14: The vertical velocity fields of optimized prediction and reality for t = 25 (left) and 400 (right).

## Conclusions

This study focused on flow prediction of von Kármán vortex street by machine learning application. Particle image velocimetry of the flow around a cylinder was carried out in a water channel for Re = 900 and recording frequencies of 400, 100, 50, 25, and 12.5 Hz resulting in a wide variety of different temporal resolutions of the applied data. POD analysis was applied to the experimental results for data reduction, and flow was cut out for the first hundred modes with the highest energies. Then, an echo state network model with 3000 neurons was fed by the data with 50 Hz frequency for 700 training time steps. Finally, the echo state network was optimized with respect to its three most influential hyperparameters: leaking rate, input scaling, and spectral radius. The vertical velocity direction prediction was preferred as the selection parameter for the network optimization. The optimization resulted in input scal-


GALA e.V., Karlsruhe, Germany, ISBN 978-3-9816764-7-1

ing = 3, spectral radius = 0.97, and leaking rate = 0.95. Qualitatively, the optimized set predicted the flow well. Meaning that it could imitate the vortex shedding process in the flow for the entire testing process of 700 time steps. However, from a quantitative point of view the predictions are not satisfactory. Thus, further investigations are planned for the optimization of other hyperparameters to enhance the predictions. Meanwhile, more efficient prediction selection parameters should be defined for flow assessment. Later, the influence of data frequency and training length will be investigated as well, and we will try to apply the optimized echo state model to different flow fields other than the von Kármán vortex street.

## References


**Pandey, S., Schumacher, J., Sreenivasan, K.,** 2020: A perspective on machine learning in turbulent flows, Journal of Turbulence, 21:9-10, 567-584

**Lienhard., J. H.,** 1966: Synopsis of lift, drag, and vortex frequency data for rigid circular cylinders. Technical report, Washington State University. Bulletin 300

**Rabault, J., Reglade, U., Cerardi, N., Kuchta, M., Jensen, A.,** 2018: Deep reinforcement learning achieves flow control of the 2D Kármán vortex street, arXiv preprint, arXiv:1808.10754

**Schena, L.,** 2021: Learning from the von Kármán Vortex Street**,** Thesis, Politecnico di Torino and von Karman Institute for Fluid Dynamics

**Morast, A.,** 2019: Implementation and comparative analysis of machine learning methods for the closed-loop control of fluid flows**,** Thesis, South Dakota School of Mines and Technology

**Arntzen, S.,** 2019: Prediction of flow-fields by combining high-fidelity CFD data and Machine Learning algorithms**,** Thesis, TU Delft

**Heyder, F., Schumacher, J.,** 2021: Echo State Network for two-dimensional turbulent moist Rayleigh-Bénard convection, Physical Review E 103 (5), 053107

**Kostas, D., Soria, J., Chong, M.S.,** 2005: A comparison between snapshot POD analysis of PIV velocity and vorticity data, Experiments in Fluids 38, 146–160

**Cierpka, C., Weier, T., Gerbeth G.,** 2010: Synchronized force and particle image velocimetry measurements on a NACA 0015 in poststall under control of time periodic electromagnetic forcing, Physics of Fluids 22, 075109

**Lukoševičius, M.,** 2012: A Practical Guide to Applying Echo State Networks, In: Montavon G., Orr G.B., Müller KR. (eds) Neural Networks: Tricks of the Trade. Lecture Notes in Computer Science, vol 7700, 659-686

**Pandey, S., Schumacher,** 2020: Reservoir computing model of two-dimensional turbulent convection, Physical Review Fluids 5, 113506



GALA e.V., Karlsruhe, Germany, ISBN 978-3-9816764-7-1